Astron. Astrophys. 341, 86–97 (1999)

ASTRONOMY AND ASTROPHYSICS

# The local stellar velocity distribution of the Galaxy⋆

## Galactic structure and potential

**O. Bienaymé**

CDS, Observatoire Astronomique de Strasbourg, 11 rue de l'Université, F-67000 Strasbourg, France

Received 18 June 1998 / Accepted 2 October 1998

**Abstract.** The velocity distribution of neighbouring stars is deduced from the Hipparcos proper motions. We have used a classical Schwarzschild decomposition and also developed a dynamical model for quasi-exponential stellar discs. This model is a 3-D derivation of Shu's model in the framework of Stäckel potentials with three integrals of motion.

We determine the solar motion relative to the local standard of rest (LSR) ($U_\odot = 9.7 \pm 0.3\,\mathrm{km\,s^{-1}}$, $V_\odot = 5.2 \pm 1.0\,\mathrm{km\,s^{-1}}$ and $W_\odot = 6.7 \pm 0.2\,\mathrm{km\,s^{-1}}$), the density and kinematic radial gradients, as well as the local slope of the velocity curve. We find out that the scale density length of the Galaxy is $1.8 \pm 0.2\,\mathrm{kpc}$. We measure a large kinematic scale length for blue (young) stars, $R_{\sigma_r} = 17 \pm 4\,\mathrm{kpc}$, while for red stars (predominantly old) we find $R_{\sigma_r} = 9.7 \pm 0.8\,\mathrm{kpc}$ (or $R_{\sigma_r^2} = 4.8 \pm 0.4\,\mathrm{kpc}$).

From the stellar disc dynamical model, we determine explicitly the link between the tangential-vertical velocity $(v_\theta, v_z)$ coupling and the local shape of the potential. Using a restricted sample of 3-D velocity data, we measure $z_o$, the focus of the spheroidal coordinate system defining the best fitted Stäckel potential. The parameter $z_o$ is related to the tilt of the velocity ellipsoid and more fundamentally to the mass gradient in the galactic disc. This parameter is found to be $5.7 \pm 1.4\,\mathrm{kpc}$. This implies that the galactic potential is not extremely flat and that the dark matter component is not confined in the galactic plane.

**Key words:** stars: kinematics – Galaxy: fundamental parameters – Galaxy: kinematics and dynamics – Galaxy: solar neighbourhood – Galaxy: structure – cosmology: dark matter

### 1. Introduction

The Hipparcos proper motion measurements (ESA, 1997) of neighbouring stars radically enlarge the size and quality of kinematical unbiased samples and provide a new opportunity to reconsider the local galactic structure and solar neighbourhood kinematics. Visualization and analysis of the local velocity field from the Hipparcos tangential velocities (Chereul et al., 1997, 1998) or combined with radial velocities (Figueras et al., 1997) show the large structuring of phase space and reveal the process of phase mixing with time. Clearly a much better understanding of the local kinematics and of the galactic dynamics will be obtained while the real complexity of the local kinematics is now apparent.

In this paper, we re-examine the classical kinematic analysis. We focus this study on the two following points: 1) it is necessary to build a dynamically coherent model of the kinematics since an analysis based on the Jeans equations is not sufficient and a more rigorous approach follows from using solutions of the Boltzmann equation; 2) we measure the galactic gradients (stellar density and kinematics, slope of velocity curve) from the local kinematic data and constrain the potential shape and the radial forces close to the plane. We deduce the flattening of the galactic potential (and mass distribution) in the Galaxy. This is a complementary approach to the more classical $K_z$ problem, i.e. the analysis of the force perpendicular to the galactic plane (Crézé et al., 1998).

In this paper, we analyse the Hipparcos proper motions, first using only a Schwarzschild decomposition (Sect. 2) then with the help of a 3D dynamical galactic model (Sect. 3) which is a generalization of Shu's model. Conclusions regarding the solar motion relative to the local standard of rest (LSR), density and kinematic gradients are drawn (Sect. 4). We finally present a first observational constraint on the radial potential bending at the solar position (Sect. 5).

### 2. Kinematic data

The Hipparcos data allow us to build a kinematic sample free from kinematic bias, that is the properties used to define the sample are not a kinematic parameter or do not explicitly depend on velocities. Survey stars, labeled S on column H68 in HIP catalogue (ESA, 1997), satisfy this criteria. They define a magnitude limited sample from HIC (ESA, 1992) magnitudes with dependence on galactic latitude, $V \leq A + 1.1 \sin|b|$, with $A = 7.9$ for spectral types earlier or equal to $G5$ and $A = 7.3$ otherwise.

A first sample has been defined with Survey stars by removing spectroscopic binaries (flag H59 set) and potential binaries in the Hipparcos solution (flag H61 set to S) and keeping stars with relative errors on parallaxes smaller than 10% to avoid

*Send offprint requests to*: O. Bienaymé

⋆ Based on data from the Hipparcos astrometry satellite

**Table 1.** Velocity dispersions ( $\mathrm{km\ s^{-1}}$) and vertex deviation (degree) for the twenty stellar groups. Colour bins 1 to 18 have 500 stars, the $19^{th}$ 477 and giants groups, the $20^{th}$, 2208 stars.

| bin | $\langle B-V\rangle$ | $\sigma_U$ | $\sigma_V$ | $\sigma_W$ | $vertex$ |
|---|---|---|---|---|---|
| 1 | $-0.05$ | 11.1 | 9.0 | 5.2 | 29.2 |
| 2 | 0.07 | 16.1 | 10.5 | 5.5 | 26.9 |
| 3 | 0.16 | 18.9 | 8.2 | 7.2 | 26.9 |
| 4 | 0.23 | 19.2 | 10.5 | 8.2 | 24.1 |
| 5 | 0.30 | 21.3 | 10.4 | 7.8 | 22.3 |
| 6 | 0.35 | 22.6 | 10.7 | 9.5 | 18.3 |
| 7 | 0.39 | 22.2 | 12.9 | 9.0 | 17.2 |
| 8 | 0.42 | 23.9 | 12.5 | 11.4 | 15.5 |
| 9 | 0.44 | 26.8 | 14.3 | 13.6 | 12.6 |
| 10 | 0.47 | 26.0 | 17.3 | 10.4 | 4.0 |
| 11 | 0.49 | 29.2 | 16.6 | 14.0 | 5.2 |
| 12 | 0.51 | 28.5 | 17.3 | 13.4 | 9.2 |
| 13 | 0.53 | 30.9 | 18.3 | 15.4 | 1.1 |
| 14 | 0.55 | 30.4 | 19.1 | 14.6 | 13.2 |
| 15 | 0.58 | 33.6 | 21.6 | 19.5 | $-2.3$ |
| 16 | 0.61 | 36.7 | 21.2 | 22.6 | 10.3 |
| 17 | 0.64 | 36.9 | 22.2 | 20.2 | 7.4 |
| 18 | 0.67 | 36.2 | 23.7 | 19.3 | 2.3 |
| 19 | 1.00 | 34.8 | 23.5 | 17.2 | 13.2 |
| 20 | giants | 34.4 | 23.8 | 17.7 | 9.2 |

kinematics containing erroneous or additional motions. The resulting sample (11766 stars) has been divided into 19 sets corresponding to successive ranges of $B-V$ colour for main sequence stars, and a twentieth set for giants in order to examine the kinematic variations between the subsets.

We have used the proper motions and parallaxes giving the tangential velocities to probe the local kinematics. Correction for galactic rotation has been applied using Feast & Whitelock's (1997) values as done by Binney et al. (1997).

We also analysed a second sample in order to use the three components of velocity, adding radial velocity measurements to the tangential velocities, and expecting to obtain a stronger constraint on the galactic structure. However, it is known that radial velocities have been measured preferentially for high proper motion stars (see Fig. 2 from Binney et al., 1997) and, as a consequence, without careful selection or analysis, such data may introduce kinematic bias. That reason alone justifies the necessity to analyse firstly the Hipparcos proper motions without radial velocities.

In order to analyze the full three kinematic components, $v_r,\ v_\theta,\ v_z$, we have used stars from the McCormick survey (Vyssotsky, 1963). This sample (895 stars) is based on spectroscopic surveys of identification of M dwarfs and must be without kinematic bias (Weiss & Upgren, 1995). Radial velocities are obtained from the literature; most data were found in the following catalogues: HIC (ESA, 1992), and more recently in Kamper et al. (1997), Reid et al. (1995), Upgren & Harlow (1996). The Simbad data base has allowed for a systematic search and cross-identifications. Keeping only data for which velocity accuracy is better than $10\,\mathrm{km\ s^{-1}}$ and rejecting identified spectroscopic binaries and variables, we obtain a sample of 309 stars. These stars have kinematics slightly hotter than the sample of giants. They have been combined to a sample of giants and red stars from HIP survey stars.

### *2.1. Preliminary analysis*

To understand the main behaviour of the distribution function $f(u,v,w)$ for the various stellar samples, we refer to the analysis given by Chereul et al. (1997, 1998), Gómez et al. (1997), Figueras et al. (1997), Binney et al. (1997), Dehnen (1998), giving both the axis ratio of velocity distributions and descriptions of clumps in phase space and irregularities. We have proceeded to a Schwarzschild distribution fitting (more exactly to a 3D gaussian fitting with one of the principal axes fixed to z axis) to the Hipparcos proper motions and $(l,b)$ coordinates distribution[1].

Table 1 and Figs. 1–3 give results for each colour bin. U is the velocity towards the Galactic center, V towards the Galactic rotation and W towards the north Galactic pole. Fitting with two ellipsoids does not improve the determination, the second fitted ellipsoid adjusting one of the moving group. We find the solar velocity relative to the local standard of rest (LSR) to be $U_\odot = 9.90 \pm 0.20\,\mathrm{km\ s^{-1}}$ and $W_\odot = 7.05 \pm 0.10\,\mathrm{km\ s^{-1}}$. The $V_\odot$ component is usually taken as the limit $\sigma_u^2 \to 0$ in the asymmetric drift relation (Fig. 3). However the slope is not constant and the limit may range between 4 and $8\,\mathrm{km\ s^{-1}}$ depending heavily on the range of $\sigma_u^2$ variances selected. The fact that the asymmetric drift relation is not linear cannot be related to the $\sigma_w/\sigma_u$ variation that is too small. The simplest explanations should be that the density or the kinematic scale lengths change gradually with populations or that the bluest populations are not kinematically relaxed. Such features are also marginally visible in Fig. 1 given by Mayor (1974).

The vertex deviation is maximum for blue stars (27°) and for the reddest stars it fluctuates around 6°. Since red stars are a mixture of old and young stars with a large vertex deviation, it is compatible with a null vertex deviation for the old stars. Accurate ages help in answering this question and show a null deviation (Gómez et al., 1997).

The velocity ellipsoid axis ratio $\sigma_w/\sigma_u$ varies rapidly with colour bins, increasing from 0.45 for blue stars to 0.55 to red ones, similar to the feature obtained by Gómez et al. (1997) by splitting stars by age intervals.

[1] A similar analysis has been done by Dehnen & Binney (1998) who use a closed form to invert the Hipparcos tangential motions into mean solar velocity and velocity dispersions. The clear advantage of their method is to avoid any prior on the underlying velocity distributions (Gaussian for instance). While our classical Gaussian fitting give *mean velocities* of stellar groups close to the values they obtain, we obtain different results concerning the *dispersions*. Performing numerical simulations we find that their method introduces a bias on estimated dispersions. The bias increases with the ratio of the mean velocity to the dispersion and cannot be neglected for the $\sigma_v$ dispersions.

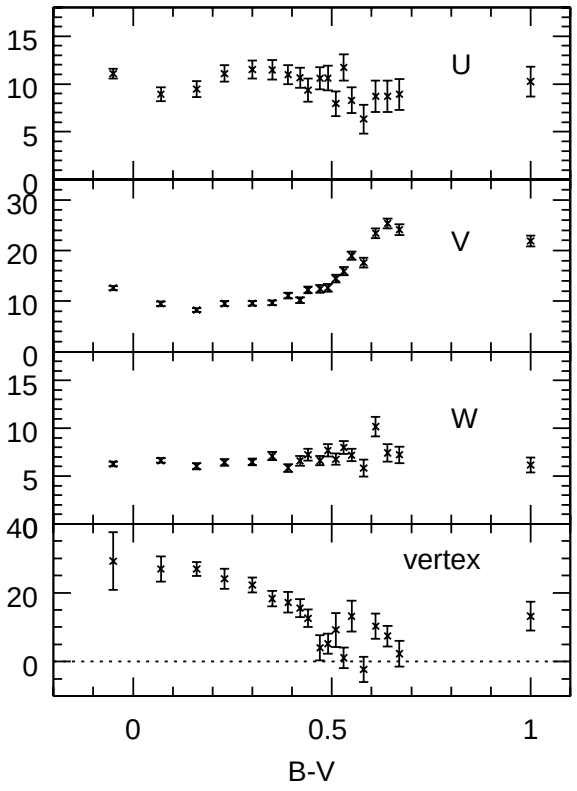


**Fig. 1.** Mean velocity ( $\mathrm{km\ s^{-1}}$) and vertex deviation dependences on stellar groups in colour bins.

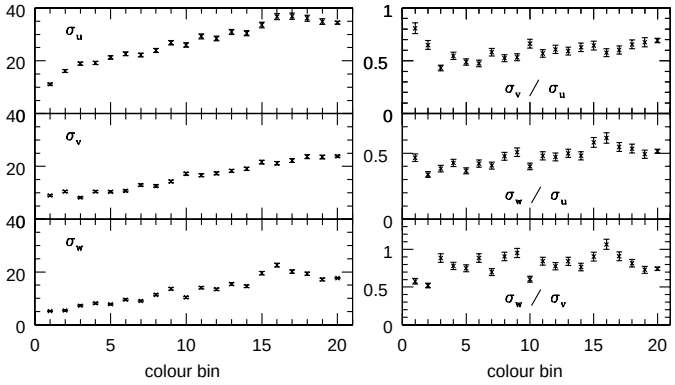


**Fig. 2.** Velocity dispersions and ratios.

### *2.2. Model fitting, parameter estimates and errors*

The Schwarzschild distribution in this section and the dynamical models in next ones represent velocity distribution functions $f(v_r, v_\theta, v_z)$ for stellar disc populations. The predicted tangential velocities distribution $f(l, b; T_l, T_b)$ as a function of galactic coordinates $l, b$ and tangential velocities $T_l, T_b$ are easily deduced. Stars with extreme velocities larger than 3 times the mean dispersions have been rejected (11685 stars remaining). This allows for the removal of possible halo stars or objects that could not be described by our disc star modeling. All models are fitted to data by adjusting the model parameters by a maximum likelihood. This means that the fitting procedure gives unbiased estimates of the model parameters (and is asymptotically convergent) *if* the observations are drawn from a parent distribution corresponding to the assumed model. Errors are obtained from the second derivatives of the likelihood at the position of maximum. The inverse of this matrix is the covariance matrix of the derived parameters giving errors and correlations. The estimated errors have also been checked by repeating fits to random subsamples.

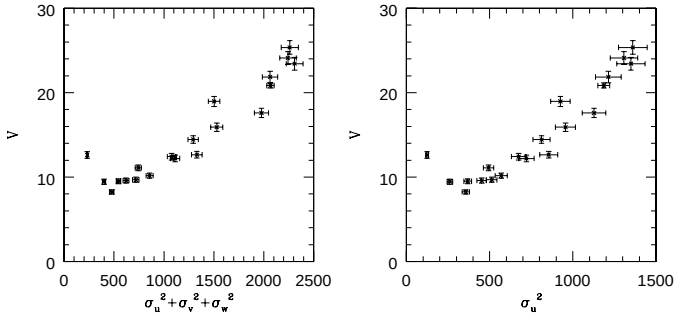


**Fig. 3.** Tangential velocity drift versus velocity variance.

Thus errors on parameter estimates are dominated by the data sampling. A much smaller source of errors comes from the accuracy of proper motions and distances measured by Hipparcos. A crude estimate of such errors is obtained by considering the median error on tangential velocities (from proper motions, parallaxes and their respective errors within our sample) and we find $1.3\,\mathrm{km\ s^{-1}}$ for one velocity component. With a sample of 11 600 stars, the resulting error, for instance, on each solar velocity component is only $0.01\,\mathrm{km\ s^{-1}}$. On the other hand, systematic effects, such as correlations between the Hipparcos solutions for close stars, exist while at large scale they must be null at the exception of the error related to the link to an inertial reference system. The deviation from inertial, non-rotating within $\pm 0.25\,\mathrm{mas/yr}$ (Kovalevsky et al., 1997), has negligible effects on the estimate of moments.

Systematic errors or bias due to the inadequacy of the model are naturally the most difficult to evaluate. Only a more general model would help to quantify that question. For instance the non-zero vertex deviation is not considered by Eq. 1 the axisymmetric model (a non-axisymmetric model with three integrals could have been considered, but in the case of a Stäckel potential, the vertex deviation would have been the same for all stellar groups). Certainly the vertex deviation introduces a bias on the estimate of velocity moments if the moments are estimated assuming a null-deviation. This will result in a bias on the other estimated parameters, scale length, slope of the rotation curve and is discussed further.

A non-parametric approach could seem more attractive, avoiding the bias of parametric models and allowing for a possibly unbiased determination of the various velocity moments. However, in this paper, we want to avoid a direct determination of the velocity moments and then the use of relations drawn from Jeans equations since we have shown that such equations lead to bias (see Sect. 3.2 and Bienaymé & Séchaud 1997, see also Kuijken & Tremaine, 1991) and that a more rigorous approach is achieved using solutions of the Boltzmann equation.

## 3. Kinematic model of galactic stellar discs

The following analysis is based on a parametric model for an axisymmetric thin rotating stellar disk. Such model was firstly introduced by Shu (1969) and extended in Bienaymé & Séchaud (1997) adding independent gradients for the density and the kinematics (see also Kuijken & Dubinski, 1995). This model is a parametric distribution function having a two-integral of motion dependence, the energy $E$ and the angular momentum $L_z$. The fundamental parameters are closely linked to the radial density gradients of the disc stellar populations and also to their kinematic gradients and to the shape of the circular velocity curve. It has been applied to the analysis of the CNS3 (Gliese & Jahreiss 1991) in order to explain the observed local velocity distribution (Bienaymé & Séchaud, 1997).

The main improvement of this model compared to Shu's model is its ability to reproduce the observed marginal velocity distribution of stars. This is due to the introduction of three realistic independent parameters, the density, kinematic dispersion and rotation curve gradients (see also previous investigations of the local kinematics with dynamically coherent distribution functions by Kuijken & Tremaine, 1991, Evans & Collett, 1993 and Cuddeford & Binney 1994).

Based on an application of the Jeans equation, Fux & Martinet (1994) deduced from the observed moments (asymmetric drift and velocity dispersions) that the density scale length is close to $2.5 - 3.0\,\mathrm{kpc}$ with assumptions on the closure of the hierarchy of velocity moment equations (Cuddeford & Amendt, 1992). We must however notice that such analysis using first and second order moments of the distribution neglects available information like the velocity distribution kurtosis and skewness.

The galactic potential can be fitted by a Stäckel potential in the solar neighbourhood. There the effective potential can be expanded in powers of (r-$R_0$) and z. How well can this expansion be matched by a similar one for a separable potential? For instance, a first order development gives a $r$ and $z$ separable potential which is then used for the estimate of the force perpendicular to the plane and for the mass density determination in the plane. Van de Hulst (1962) and Kent & de Zeeuw (1994) solved the expansion problem with Stäckel potentials. The expansion includes the third order term $rz^2$ related to the potential flattening. If the galactic potential were of Stäckel form we would have an exact measure of its flattening (through the parameter $z_0$, the focus of the ellipsoidal coordinate system defined in the Appendix). The galactic potential is certainly not exactly of a Stäckel form, but probably not so far from it as long as like here, we consider stars within a small range of excursion from the solar position ($3\,\mathrm{kpc}$ radially and $1\,\mathrm{kpc}$ vertically). A more general analysis (using orbit computations for instance) could establish accurately the coupling between the vertical and radial motions and its link to any potential. The advantage of Stäckel potentials is their tractability and they are certainly sufficient for a first analysis. In this paper it allows us to establish formally the importance of the potential flattening on the stellar motions in the solar neighbourhood.

### 3.1. 3D axisymmetric stellar disc kinematic model

The model is a 3D extension of the 2D distribution function described in Bienaymé & Séchaud (1997). This model is defined in 3D axisymmetric Stäckel potentials where three integrals of motion are known ($E, L_z, I_3$). Being a function of these three integrals, $f(E, L_z, I_3)$ is a stationary solution of the collisionless Boltzmann equation. It is also close to the Schwarzschild distribution for small velocity dispersions and its associated density is nearly exponential as are the kinematic radial distributions.

The expression of the distribution function is given by (see also the Appendix for more details):

$$f(E,L_z,I_3) = \frac{2\Omega(R_c)}{2\pi\kappa(R_c)}\frac{\Sigma(L_z)}{\sigma_r^2(L_z)}\exp\left[-\frac{E-E_{circ}}{\sigma_r^2}\right] \frac{1}{\sqrt{2\pi}}\frac{1}{\sigma_z(L_z)} exp\left[-(\frac{R_c(L_z)^2}{z_o^2}+1)^{-1}(\frac{1}{\sigma_z^2}-\frac{1}{\sigma_r^2})I_3\right] \quad (1)$$

and is null when $L_z < 0$, where $R_c = R_c(L_z)$ is the radius of circular orbit stars with angular momentum $L_z$ and having the energy $E_{circ}(R_c)$. $\Omega$ is the angular velocity, $\kappa$ the epicyclic frequency and

$$\Sigma(L_z) = \Sigma_0 \exp[-R_c(L_z)/R_\Sigma] \quad (2)$$

$$\sigma_r(L_z) = \sigma_{0,r} \exp[-R_c(L_z)/R_{\sigma_r}]. \quad (3)$$

$$\sigma_z(L_z) = \sigma_{0,z} \exp[-R_c(L_z)/R_{\sigma_z}]\,, \quad (4)$$

in the following, we put $R_{\sigma_z} = R_{\sigma_r}$ and we define the radial dependence of the potential in the galactic plane assuming a power law rotation curve $v_c(r) \sim r^\alpha$.

### 3.2. Some properties

For a convenient range of parameters ($R_\Sigma$, $R_{\sigma_r}$), such a distribution has effectively nearly exponential density and kinematic decreases with respective scale lengths close to $R_\Sigma$ and $R_{\sigma_r}$ (Fig. 4). Models with extremely large velocity dispersions cannot have small scale lengths (i.e. large density gradients). In such cases, the effective density scale lengths are different from the input parameter $R_\Sigma$ and such models no longer have an exponential decrease over a large range of radius (Fig. 4). Analysing the Hipparcos data, we will not be concerned by this problem since the velocity dispersions involved in the data are small.

The asymmetric drift (AD) relates the velocity dispersion of any stellar group to its tangential drift. A quite general form is given by Binney & Tremaine, 1987 (BT) (Eq. 4.34), valid in the galactic plane at $z = 0$, relating linearly $V_{AD}$ to the variance $\sigma_r^2$ (for constant dispersion ratios and kinematic scale length that is independent of stellar types). That equation can be considered as a first order development with a limited range of validity. We have computed the asymmetric drift relation for stationary solutions given by our model and the results are plotted (Fig. 5) for different sets of parameters. The AD relation is found to be nearly linear in the range of drift from $0$ to $30\,\mathrm{km\ s^{-1}}$. This interval is apparently the range of validity of the classical equation.

Hipparcos data as well as other data used to study the asymmetric drift fall in this range of velocity drift. However, as seen

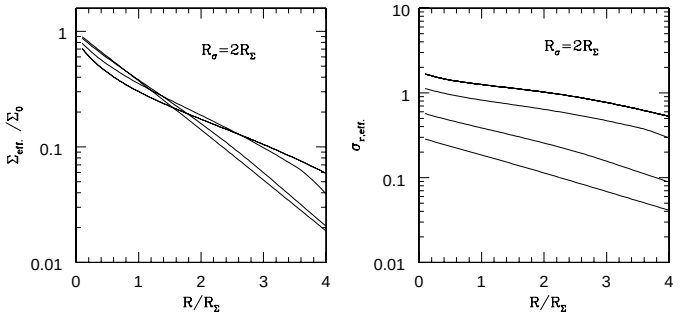


**Fig. 4.** Effective density and radial velocity dispersion computed from the corresponding moments of the distribution function Eq. 1 (models computed with $z_o = \infty$ and a flat rotation curve $v_c(r) = 1$, $\sigma_{r,eff}$ are plotted in the same units). Four radial density distributions with $R_\sigma = 2R_\Sigma$ and $\sigma_0 = .3 - .6 - 1.2 - 1.8$ are plotted. Solar position is at $R_0/R_\Sigma = 2.5 - 3.5$ and $\sigma_r(R_0/R_\Sigma) = 0.3$ for the thick disc. Above a critical $\sigma_0$ value, the density scale length increases and is no longer close to $R_\Sigma$.

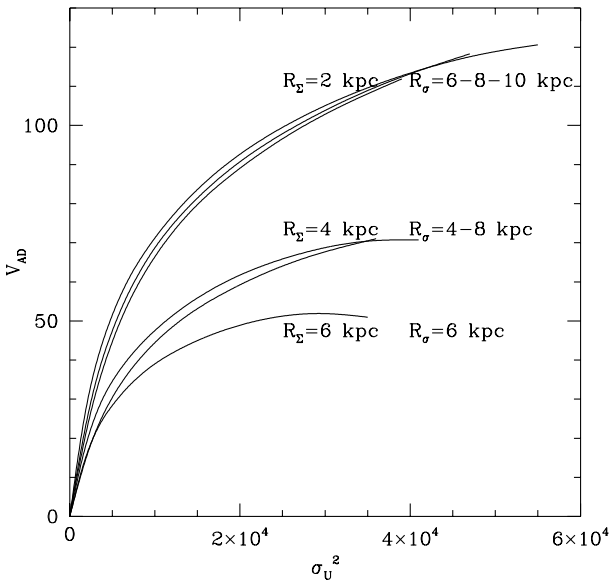


**Fig. 5.** Asymmetric drift relations. Tangential velocity drift versus radial velocity variance for models with various density and kinematic gradients ($R_0 = 8.5\,\mathrm{kpc}$, $V_0 = 220\,\mathrm{km\,s^{-1}}$). Models with the largest density scale length present a saturation effect on the amplitude of the tangential velocity drift.

in Sect. 2.1, the asymmetric drift relation is not strictly linear. Finally for stellar populations having larger drifts, like the thick disc, the use of a linear relation is certainly wrong.

The asymmetric drift is neither entirely described by the moment equation 4.34 of Binney & Tremaine (1987) nor by the more exact relations such these plotted on Fig. 5 since, in some range of drift, different modeling may have similar AD relations. Higher moments or marginal velocity distributions help to identify and discriminate between models. This is recognized in Fig. 6 where various signatures, like drift but also kurtosis and skewness of the $v_\theta$ distributions, are identifiable. Differences due to a short or a long scale length are visible. In the case of the shortest scale length $1.8\,\mathrm{kpc}$, with $\sigma_r$ increasing, $f(v_\theta)$ stays symmetric and the maximum shifts regularly. For larger scale length $2.5\,\mathrm{kpc}$, the $f(v_\theta)$ distribution becomes highly asymmetric. At higher scale length $4.5\,\mathrm{kpc}$, the maximum of the $v_\theta$ distributions is nearly not shifted.

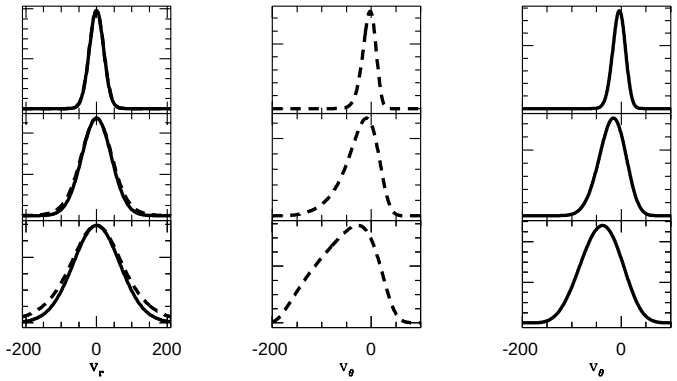


**Fig. 6.** Marginal velocity distributions at solar position, for two models with short (full lines) and long (dashed lines) density scale lengths. Top to bottom with increasing velocity dispersions. Left: radial velocity distribution for both models, middle: tangential velocity distribution for model with $R_\Sigma = 2.5\,\mathrm{kpc}$, $\mathrm{R}_\sigma = 7.5\,\mathrm{kpc}$, right: for model with $R_\Sigma = 1.8\,\mathrm{kpc}$ $\mathrm{R}_\sigma = 15\,\mathrm{kpc}$.

### 3.3. $f(E, L_z, I_3)$ at $z = 0$

We give, below, the simpler expressions of the distribution function in the galactic plane ($z = 0$) (see Appendix) corresponding closer to the situation of the Hipparcos sample we are analysing. We have:

$$f(E, L_z, I_3) = g(r; \dot{r}, \dot{\theta}) f_\perp(r, z; \dot{\theta}, \dot{z}) \tag{5}$$

with

$$f_\perp = \exp\left\{-\frac{\dot{z}^2}{2}\left[\frac{1}{\sigma_r^2} + (\frac{1}{\sigma_z^2} - \frac{1}{\sigma_r^2})\left(\frac{r^2 + z_o^2}{R_c(L_z)^2 + z_o^2}\right)\right]\right\} \tag{6}$$

where $z_o$ (defined in Appendix as the focus of the ellipsoidal coordinate system) is related to the shape of a Stäckel potential.

For a flat rotation curve with $v_c(r) = v_o$

$$f_\perp = \exp\left\{-\frac{\dot{z}^2}{2}\left[\frac{1}{\sigma_r^2} + (\frac{1}{\sigma_z^2} - \frac{1}{\sigma_r^2})\left(\frac{r^2 v_o^2 + z_o^2 v_o^2}{r^2 v_\theta^2 + z_o^2 v_o^2}\right)\right]\right\}. \tag{7}$$

This $v_\theta$, $v_z$ coupling is established only in the case of a Stäckel potential and of a quasi-exponential stellar disc. Different couplings would have been obtained if we had considered another density distribution.

Towards $z_o = \infty$, the potential is cylindrical and

$$f_\perp = \exp\left\{-\frac{\dot{z}^2}{2\sigma_z^2}\right\}. \tag{8}$$

Towards $z_o = 0$, the potential is spherical and

$$f_\perp = \exp\left\{-\frac{\dot{z}^2}{2\sigma_z^2}\left[\frac{\sigma_z^2}{\sigma_r^2} + (1 - \frac{\sigma_z^2}{\sigma_r^2})\frac{v_o^2}{v_\theta^2}\right]\right\}. \tag{9}$$

Dependence on the $z_o$ parameter is easily identifiable and can be isolated from the other parameter dependencies. This is

**Table 2.** Solar motion relative to the LSR and galactic characteristics deduced from the local stellar kinematics (1-$\sigma$ errors). Best estimates of parameters are shown for two ranges of data (2 to 20 and 3 to 20 bins) and with models with one kinematic scale length $R_{\sigma_r}$ or with two differents scales for blue and red stars. Typical errors are given in the last column but do not include the correlations. Except for $u_\odot$ and $w_\odot$, they are raised by a factor $\sim 1.5-2$ when correlations are considered.

| | bins 2−20 one $R_{\sigma_r}$ | bins 3−20 one $R_{\sigma_r}$ | bins 2−20 two $R_{\sigma_r}$ | bins 3−20 two $R_{\sigma_r}$ |
|---|---|---|---|---|
| $u_\odot$ | 9.5 | 9.5 | 9.6 | $9.7 \pm .3$ |
| $v_\odot$ | 3.8 | 3.5 | 5.2 | $5.2 \pm .5$ |
| $w_\odot$ | 6.7 | 6.7 | 6.7 | $6.7 \pm .2$ |
| $R_\Sigma$ | 1.5 | 1.5 | 1.7 | $1.8 \pm .1$ |
| $R_{\sigma_r}$ | 10.0 | 10.0 | 9.3 & 19 | $9.7 \pm .4$ & $17 \pm 2$ |
| $\alpha$ | $-.22$ | $-.24$ | $-.22$ | $-.24 \pm .02$ |
| $z_o$ | 19 | 17 | 23 | $24 \pm 10$ |

discussed in Sect. 5 and in the Appendix. This dependence links the velocity distribution to the potential, bringing a constraint on the galactic mass distribution.

## 4. Model versus data: solar motion and galactic scale lengths

Model to data comparison is achieved by splitting the stellar sample by colour intervals covering various ranges of kinematics. The ratio between the widths of the marginal distribution in $v_r$ to $v_\theta$ is mainly linked to the slope of the rotation curve, while the shape of the $v_\theta$ marginal distribution is strongly correlated to the scale lengths. The exact combination of these correlations is untangled by fitting the model distribution (Eq. 1) to the observed velocity distributions.

### *4.1. Results of model fitting to Hipparcos tangential velocities*

Results are given in Table 2. For each colour bin we adjust one distribution function (Eq. 1) with the common free parameters for all colour bins being the solar motion, $R_\Sigma$, $R_{\sigma_r}$, $\alpha$ (logarithmic slope of the rotation curve) and $z_o$. Parameters not given in Table 2 are the radial and vertical velocity dispersions associated to each colour bin.

We find that the determination of the tangential solar velocity $v_\odot$ is sensitive to the first colour bin (youngest stars) that we have rejected. The density scale length is also correlated to the solar velocity $v_\odot$. All the results favour a short scale length.

Since the AD relation is not linear (Fig. 3), it is very natural to consider that the $R_\Sigma$, $R_{\sigma_r}$ parameters are not the same for all stellar populations. The change of the ellipsoid axis ratio cannot explain the bending of the AD relation. In external galaxies the change with colour of the density scale length is only about 20% (de Jong, 1996). However the youngest stars may have a smaller density scale length close to the ISM one, though it also depends on the SFR radial dependence. More certain, the kinematic scale length of youngest populations must be close to the ISM kinematics with a nearly null gradient. The different rate of dynamical heating with radius should change the kinematics to the observed one for old populations. For these reasons, we have tried a modeling with different kinematic scale lengths for the bluest stars (bins 3-10) and for the reddest stars (bins 11-20). The likelihood is improved; we find out $v_\odot = 5.2\,\mathrm{km\ s^{-1}}$ and the density scale length $1.8\,\mathrm{kpc}$. We find for the bluest stars a nearly null kinematic gradient, in accordance to our expectation, and for reddest stars $R_{\sigma_r}$ is $9.7\,\mathrm{kpc}$ (or $R_{\sigma_r^2} = 4.9\,\mathrm{kpc}$) close to the Lewis & Freeman's value (1989) $R_{\sigma_r^2} = 4.4\,\mathrm{kpc}$ based on 600 giants towards the centre and anticentre directions.

The comparison of the maximum likelihood (ML) of respective models allows us to determine their relative goodness of fit: the likelihood ratio test giving a measure of the reliability of adding new parameters. The likelihood-ratio statistics (Nemec & Nemec 1991, Kendall & Stuart 1967) is $\lambda = \frac{\mathcal{L}_1}{\mathcal{L}_2}$ where $\mathcal{L}_1$ is the likelihood for models based on $K_1$ components. Models with a larger number of components $K_2$ may give a better fit with $\lambda$ smaller than one. The statistical significance of $\lambda$ is obtained by comparing $-2\log\lambda$ to the upper percentile of a $\chi^2$ distribution with the number of degrees of freedom equal to the difference in the number of parameters between the two models. (However, these results only hold if the asymptotic normality and efficiency of the ML estimator are satisfied, Kendall & Stuart, 1967).

Likelihoods of the discussed models are summarized in Table 3. Summarizing:

1) We find that Gaussian fits are significantly improved when the vertex is adjusted ($\lambda \sim 220$ for $\sim 20$ more parameters).
2) Comparing the Gaussian fit with a non null vertex to Eq. 1 modelings, we see that the Gaussian gives a significantly improved fit (and considering they have more free adjusted parameters).
3) More interesting is that when Eq. 1 modelings are compared to the more similar Gaussian fits with null vertex, the likelihood is very significantly improved considering that the number of free parameters is lowered by about 65.
4) Finally comparing the two Eq. 1 models with one or two kinematic scale lengths, the change of likelihoods is significant (as we add one supplementary parameter, the fit is improved) ($-2\log\lambda$=5.2 and 30 for 18 and 19 bins, corresponding respectively to an improvement with a probability of 0.98 and $1. - 5 * 10^{-8}$).

Errors given in the last column of Table 2 are deduced from the diagonal of the covariance matrix. Existing correlations raise the errors. A good indicator is the global correlation coefficient (Eadie et al., 1971) a quantity that is a measure of the total amount of correlation between a variable and all the other variables (this coefficient being one if the variable is a linear combination of the other variables). Most correlations and global correlations are small except for the following variables: 1) a correlation and a global correlation about 0.8 between $v_\odot$ and $R_\Sigma$; 2) $R_{\sigma_r}$ has correlations of 0.3 and 0.5 with $v_\odot$ and $R_\Sigma$ and a global correlation of 0.8; 3) $\alpha$ has correlations of 0.2 and 0.3 with $v_\odot$ and $R_{\sigma_r}$ and a global correlation of 0.5. This means

**Table 3.** Logarithm of likelihoods of models. Likelihood ratio tests the improvement of the goodness of fits.

| models | ln ($\mathcal{L}_{bins\ 3-20}$) | Nb parameters | ln ($\mathcal{L}_{bins\ 2-20}$) | Nb parameters |
|---|---|---|---|---|
| Gaussian fit | $-93993.3$ | 126 | $-97753.3$ | 133 |
| Eq. 1: two kinematic scale lengths | $-94090.6$ | 45 | $-97872.4$ | 47 |
| Eq. 1: one kinematic scale length | $-94093.2$ | 44 | $-97887.9$ | 46 |
| gaussian fit with null vertex | $-94215.2$ | 108 | $-97992.8$ | 114 |

that errors given in Table 2 must be multiplied by $\sim 1.5-2$ for the variables $v_\odot, R_{\sigma_r}, R_\Sigma$ and $\alpha$.

The estimated density scale length is directly proportional to the adopted solar galactic radius $R_0$ (here taken as $8.5\,\mathrm{kpc}$). It also depends on the adopted $V_0$ in a less direct way. We find that a decrease of $V_0$ by 10 percent increases the estimate of $R_\Sigma$ by about 10 percent while the slope of the rotation curve is unchanged, $\alpha = -0.23$. $R_0$ and $V_0$ are not accurately known but they are linked by the determination of the $R_0/V_0$ ratio (from the Oort's constants difference $A-B$), it results that $R_\Sigma$ remains nearly unchanged by the $R_0$ and $V_0$ uncertainties.

It is worth noting that we find a decreasing rotation curve in agreement with the new determination of the Oort's constants (Feast & Whitelock, 1997, or Olling & Merrifield, 1998) ($A+B=(dV/dR)_0=-2.4\,\mathrm{km\,s^{-1}\,kpc^{-1}}$). Considering the constraints given by the rotation curve (Rohlfs et al., 1988), a decreasing rotation curve is obtained only with small $R_0$ and $V_0$ (smaller than the IAU recommended values). Olling & Merrifield (1998) find $R_0 = 7.1\,\mathrm{kpc}$ and $V_0 = 184\,\mathrm{km\ s^{-1}}$. The corresponding $\alpha$, the logarithmic slope of the rotation curve, is then $-0.10$ not in excellent agreement with our local determinations.

This difference could be partly explained by the most evident bias of our model, i.e. the assumption of a null vertex deviation that leads to biased estimates of the moments of the ellipsoidal velocity distributions. This bias can be evaluated by comparing the velocity moments determined with a non-null vertex deviation (Table 1) and those determined assuming a null deviation. The largest axis ratio estimates are changed by 10 to 5 percent for the six first bins and 0 to 3 percent for the other bins. We quantify from Eq. 4.52 and Eq. 4.35 (BT) the possible order of magnitude of the bias on the slope of the rotation. $\alpha$ could be increased by +0.1 to $-0.14$, while the estimate of scale lengths would be increased by 10 percent. Then the estimated density scale length would be $2.1\,\mathrm{kpc}$. Our bias estimation cannot be applied so simply, and we will consider that it gives at least a more realistic estimate of errors bars, much larger than the Poissonian errors.

More generally we remark that it is certainly not clear how correct the use of equations like Eqs. 4.35 or 4.52 (BT) obtained by assuming an axisymmetric galaxy is when they are applied to observed velocity distributions that do not satisfy the symmetry conditions and when the observed moments are not computed along the coordinate system. Limitation and bias in the application of our modeling (Eq. 1) are probably also present when using Jeans and the related equations.

These results are close to previous kinematic determinations of the scale lengths by Mayor (1974) ($R_\Sigma = 2.2\,\mathrm{kpc}$) or Oblak & Mayor (1987) ($R_{\sigma_r} = 10\,\mathrm{kpc}$ or $R_{\sigma_r^2} = 5\,\mathrm{kpc}$) and Fux & Martinet (1994) ($R_\Sigma = 2.5\,\mathrm{kpc}$) based on the local stellar kinematics.

The short density scale length we have determined is also in agreement with the following determination from star counts at low galactic latitudes: with IR star counts by Porcel et al. (1998) ($2.1\,\mathrm{kpc}$), Ruphy et al. (1996) ($2.3\,\mathrm{kpc}$), Kent et al. (1991) ($3.0\,\mathrm{kpc}$) and in visible by Robin et al. (1992) ($2.5\,\mathrm{kpc}$). Higher latitude star counts (in visible) like those by Siegel et al. (1997) may give a longer scale length. Could these results be biased by thick disc stars? We just mention here that the larger thick disc scale length ($3\,\mathrm{kpc}$) measured by Ojha et al. (1996) using star counts and proper motions that allow one to separate accurately the stellar populations.

Accuracy on $z_o$ is extremely low since it depends on $v_\theta$, $v_z$ coupling that is not well defined by proper motions alone. At $2\sigma$ all $z_0$ values are possible.

### *4.2. 3D velocity data*

3D velocity data have been used in order to improve the determination of $z_o$ because this parameter depends on the coupling of velocity components.

For that purpose we first tried to determine $z_o$ with a subset from the McC survey (309 stars) but the accuracy was not sufficiently improved. We augmented this sample with HIP survey stars with existing radial velocities. While McC sample is free from kinematic bias, this is not the case for Hipparcos stars with published radial velocities. However the completeness (and absence of kinematic bias) is achieved for high velocity stars (Binney et al. 1997). Since $z_o$ is exclusively constrained by the highest velocity stars and is unconstrained by stars with velocities smaller than $20\,\mathrm{km\ s^{-1}}$, we expect a small kinematic bias.

Combining in a single sample, McC stars (309), giants (1239 from bin 20) and reddest dwarfs (833 stars, $B-V>.525$) with radial velocities we find that the optimal fittings are achieved with a four-component model (i.e.: adding four elementary distributions (Eq. 1) with different weights $\Sigma_0$ and radial and vertical velocity dispersions $\sigma_{r,0}$, $\sigma_{z,0}$). Exploring the maximum likelihood space, with the parameters being free or setting the various parameters with values obtained in Table 2, we arrive at the following conclusions: with these data $R_\Sigma$, $z_o$ and $v_\odot$ are correlated and may vary in the range of models given in Table 4. The accuracy and errors are determined from the diagonal of the covariance matrix that reflects the errors due to

**Table 4.** Best fit models to the 3D stellar velocity distributions.

| $R_\Sigma$ kpc | $z_o$ kpc | $v_\odot$ km s$^{-1}$ | log of likelihood |
|---|---|---|---|
| 4.0 | $7.9 \pm 2.0$ | 12.4 | $-34.75$ |
| 2.5 | $6.9 \pm 1.4$ | 9.5 | $-31.22$ |
| 2.0 | $6.1 \pm 1.4$ | 7.8 | $-30.02$ |
| 1.7 | $5.7 \pm 1.4$ | 6.1 | $-29.64$ |
| 1.5 | $5.4 \pm 1.4$ | 5.0 | $-39.80$ |
| 1.3 | $5.0 \pm 1.4$ | 3.4 | $-30.49$ |
| 1.1 | $4.9 \pm 1.9$ | 1.3 | $-31.84$ |

the data sampling. On the other hand, varying $\alpha$ in the range -0.3 to -0.1 (with $V_\odot$ fixed) has nearly no effect on the other adjusted parameters. In fact this sample alone (hot kinematic) is suited to constrain the parameter $z_o$ but not accurately the others. Combining results from Table 4 to these obtained using HIP tangential velocities from survey stars (Table 2), where the solar velocity $v_\odot$ ranges between 4 and $6\,\mathrm{km\,s^{-1}}$, and $R_\Sigma$ about $1.8\,\mathrm{kpc}$, we deduce that $z_o$ is $5.7 \pm 1.4\,\mathrm{kpc}$.

The $z_0$ dependence on $R_0$ is such that $z_0/R_0$ does not depend on $R_0$. As a consequence the parameter $\Lambda$ (defined in Sect. 5) does not depend on $R_0$. Concerning the $V_0$ parameter, a change of 10 percent produces a negligible change of $\sim 1$ percent on $z_0$.

The vertical $R_{\sigma_w}$ and radial $R_{\sigma_r}$ kinematic scale lengths have been supposed equal because the data do not allow us to determine separately the two scale lengths. They have certainly the same (large) order of magnitude. (The kinematic radial scale length $R_{\sigma_r}$ is about 9 kpc for giants, Neese & Yoss, 1988, Lewis et Freeman 1989, a value large compared to the density scale length. For younger populations the kinematic scale length should be even larger).

Now considering the distribution function (Eq. 1), a decrease of $R_{\sigma_w}$ (at constant $R_\sigma$) has the effect of increasing the vertical dispersion for velocities smaller than $V_0$ and decreasing for velocities larger than $V_0$ (Figs. 7, 8). The apparent change on the isocontours would mimic a change of the $z_o$ parameter. We notice it also changes the velocity distribution $f(v_\theta, v_z = 0)$ and then the two effects (changes on $R_{\sigma_w}$ and $z_o$) could be distinguished. Finally, modifying independently both $R_\sigma$ and $R_{\sigma_w}$ in the range 6-15 kpc, gives a range of values for fitted $z_o$ from 3.8 to 6 kpc that is nearly about the range of the errors given by the maximum likelihood.

## 5. Local constraints on the galactic potential

In building the 3D kinematic model, we defined the parameter $z_o$ that is a measure of the radial bending of the potential. It is also tightly related to $\delta$ the vertical tilt of the velocity ellipsoid given by

$$\tan 2\delta = \frac{2\,\sigma^2_{r,z}}{\sigma^2_{r,r} - \sigma^2_{z,z}}. \qquad (10)$$

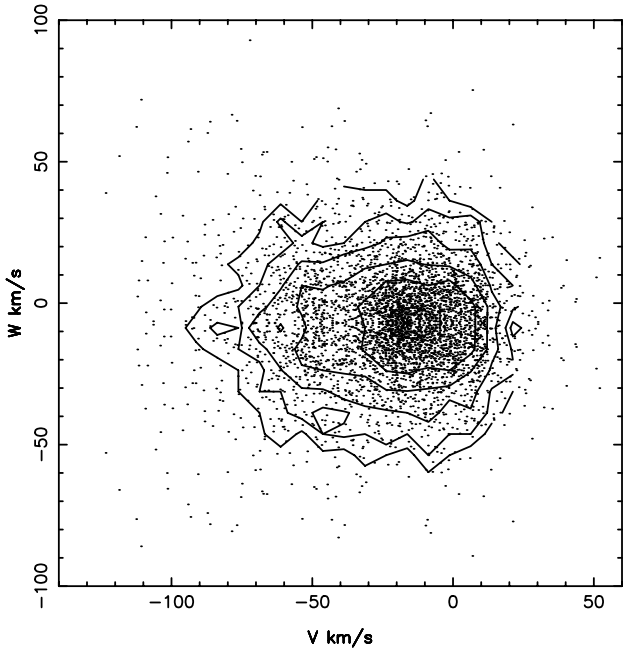


**Fig. 7.** Symmetrized (axis $w = -7\,\mathrm{km\ s^{-1}}$) observed $f(v, w)$ marginal velocity distribution. The maximum density corresponds roughly to Pleiades SuperCluster position (around v=$-22\,\mathrm{km\ s^{-1}}$, w=$-5\,\mathrm{km\,s^{-1}}$) and the innermost contour is certainly affected by non-stationary features that cannot be modeled by the stationary solution given by Eq. 1: it is the region where selection effects are present but it is also the region where data do not constrain the parameter $z_0$. We notice the egg-shape of isocontours pointing towards negative V-velocity.

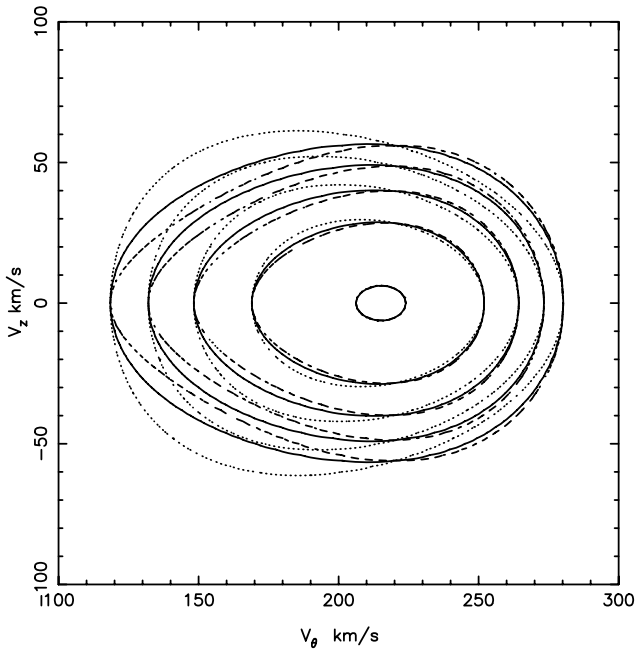


**Fig. 8.** Isocontours of the $f(v_\theta, v_z)$ distribution for three models: best fit model (continuous lines), and best fit model changing $z_o$ to 0 (dashed) and to $\infty$ (dotted). Isocontours are egg-shape, best fit and $z_0$=0 solutions pointing towards negative $V_\theta$-velocity like data isocontours (Fig. 7). $z_0 = \infty$ solution (dotted) has isocontours pointing towards positive $V_\theta$-velocity.

Hori & Liu (1963) shown that in a Stäckel potential the tilt $\delta$ depends only on the positions:

$$\tan 2\delta = \frac{2\,r\,z}{r^2 - z^2 + z_o^2}. \quad (11)$$

The change of the tilt close to the galactic plane (where $z = 0$, $\delta = 0$ and first order vertical derivatives of $\sigma_{r,r}$ and $\sigma_{z,z}$ are null) is

$$\partial_z(\tan 2\delta) = \partial_z \sigma^2_{r,z}\ \frac{2}{\sigma^2_{r,r} - \sigma^2_{z,z}} = \frac{\Lambda(r)}{r} \quad (12)$$

and for a Stäckel potential (at $z = 0$)

$$\Lambda(r) = \frac{r^2}{r^2 + z_o^2}. \quad (13)$$

A general and approximate expression valid at $z = 0$ (exact in the case of Stäckel potentials) is given by Amendt & Cuddeford (1991) (see also Cuddeford & Amendt, 1991, 1992) where $\Lambda(r)$ depends on potential derivatives:

$$\Lambda(r) = \left(\frac{r^2 \Phi_{rzz}}{3\Phi_r + r\Phi_{rr} - 4r\Phi_{zz}}\right)(r, z = 0). \quad (14)$$

They show that $\Lambda(r)$ may be strongly linked to the mass gradient in the galactic plane. For the simplest cases we have that:

1) for a spherical potential, $z_o = 0$, $\Lambda = 1$ and the velocity ellipsoid points towards the galactic center,
2) while for a cylindrical potential, $z_o = \infty$, $\Lambda = 0$ and the ellipsoid stays everywhere parallel to the galactic plane.

### *5.1. Measuring $z_o$*

We measure (Sect. 4.1) $z_o$ directly from Hipparcos data using the distribution function Eq. 1. Better constraints are obtained using a sample with 3D velocities since $z_o$ is strongly tied to the coupling between $v_\theta$ and $v_z$ components (Sect. 4.2).

Fig. 7 shows the $f(v, w)$ marginal velocity distribution for the 3D velocity sample and Fig. 8 the isocontours for three models: the first model is the best fit model ($z_o = 5.7\,\mathrm{kpc}$) and two similar models just changing $z_o$ to 0 and $\infty$. We remark that these three models are strictly identical on the two axis $f(v, w = 0)$ and $f(v = v_{circ}, w)$ (see Appendix), and that the differences are important for large velocities both in $v$ and $w$. Outside these axis, $f(v, w)$ depends quite exclusively on $z_o$. There is in fact a small dependence on $\alpha$, limited by the small range of acceptable $\alpha$ values from -.3 to -.1. There is also a dependence on the kinematic scale lengths $R_{\sigma_r}$ and $R_{\sigma_z}$ that is null when the two scales are equal and is small when the scale lengths are large which is the actual situation.

### *5.2. Constraints on the galactic potential*

Since the determination ($z_o = 5.7 \pm 1.4\,\mathrm{kpc}, \Lambda = 0.69 \pm .10$) is not yet very accurate, we have not developed detailed galactic mass models (uncertainties on $R_\sigma$ and $R_{\sigma_w}$ could lead at most to $\Lambda = 0.83$ corresponding to a more spherical potential). We mention here the main conclusions that can be drawn from the $(z_o; \Lambda)$ measure in the galactic plane (longer developments are presented in Amendt & Cuddeford, 1991).

For a galaxy with a flat rotation curve and a full flat mass distribution, $\Lambda(r) = 0.5$ in the galactic plane. For an exponential disc in a flat rotation curve potential and inside a spheroidal halo, $\Lambda(r) \simeq \frac{r}{4R_\Sigma}$ (the expression is valid at radii where the disc density remains much larger than the halo density). For a strictly spherical mass distribution $\Lambda = 1$. Combining components with different flattenings, a large range of values from 0 to 1 and more are possible.

At face value, ($z_o = 5.7\,\mathrm{kpc}, \Lambda = 0.69$) implies that the potential distribution close to the sun is not extremely flattened and that not all the galactic mass is confined inside the galactic plane.

If the galactic halo is spherical, the radial mass distribution in the disc exponential and the rotation curve flat, then we deduce from the observed $\Lambda$ that the scale length of the mass distribution in the disc is about $2.7 - 3.1\,\mathrm{kpc}$ and is smaller or larger if the rotation curve is respectively decreasing or increasing. Flattening the halo is compensated by decreasing the mass density scale length in the disc in order to keep $\Lambda$ to the observed value. However the dark matter halo cannot be flattened by more than a factor of 4 or 6, otherwise the local halo density is not much smaller than the disc mass density and then $\Lambda$ converges quickly towards 0.5.

More precise conclusions depend on adopted values of the galactic structure such as the galactic solar radius $R_0$ and also the local stellar disc and ISM mass density. The solar galactic radius $R_0$ may be smaller than the IAU recommended value (Reid, 1993). With $R_0 = 7.5\,\mathrm{kpc}$ then $\Lambda = R_0/(4R_\Sigma)$ is closer to the observed value. A smaller $R_0$ implies that the rotation curve is locally decreasing (Rohlfs & Kreitschmann, 1988) in concordance with our findings from the local velocity distribution (Table 2).

When we model potentials with a flat exponential disc and a Miyamoto halo (with a core radius and a flattening), we do not find models with a strictly spherical halo and having sufficiently small $\Lambda$ if the rotation curve is decreasing. Halos with a density scale height around $2\,\mathrm{kpc}$ at $R_0$ give the observed $\Lambda$. However this result depends critically on the slope of the rotation curve and with flat or rising curve, spherical halos (density scale height is $\sim 7\,\mathrm{kpc}$ at $R_0$) are obtained.

We conclude that an extremely flat dark halo is rejected at $2\sigma$ and models favour a spherical halo or halos with a local scale height larger than $2\,\mathrm{kpc}$ at the solar galactic radius. There is a need for more data to bring a stronger constraint and to determine more precisely the galactic potential. This is also important because the basic measured quantities are different from those determined in the classical $K_z$ problem, and consequently this new method is an independent test for measuring the mass distribution in the galactic plane.

We may reject with certainty some galactic mass distributions: those corresponding to (unexpected) oblate Stäckel po-

tentials with a focus beyond the solar galactic radius and an ellipsoid tilt pointing in the galactic plane outwards.

Models with $\Lambda = 0$ are also rejected: they could correspond to cylindrical potential produced by a vertical and extremely prolate dark matter halo with a nearly constant mass density up to height of about $10\,\mathrm{kpc}$. Such a halo would rotate about its major axis in order to have an angular momentum parallel to the stellar disk one. This is a confirmation of collisionless simulations of the dark halo that do not produce such halo configurations: "There is decided lack of halos which rotate about the major axis although this is a stable configuration" (Warren et al., 1992).

## 6. Conclusion

We analyse the kinematics of nearby stars from the Hipparcos proper motions and determine the solar motion and the kinematic and density gradients of the observed stellar populations. For that purpose, we have extended a dynamical model (Shu, 1969) for axisymmetric exponential stellar discs to 3 dimensions.

We determine the solar motion relative to the LSR to be: $U_\odot = 9.7 \pm 0.3\,\mathrm{km\ s^{-1}}$, $V_\odot = 5.2 \pm 1.0\,\mathrm{km\ s^{-1}}$ and $W_\odot = 6.7 \pm 0.2\,\mathrm{km\ s^{-1}}$.

Assuming $R_0 = 8.5\,\mathrm{kpc}$ and $V_0 = 220\,\mathrm{km\ s^{-1}}$, we determine that the stellar density scale length is short, $R_\Sigma = 1.8 \pm 0.2\,\mathrm{kpc}$.

The nonlinear shape of the asymmetric drift is more likely explained assuming different $R_{\sigma_r}$ for young and old stars. We find a large kinematic scale length for blue (young) stars $R_{\sigma_r} = 17 \pm 4\,\mathrm{kpc}$ and for red stars (predominantly old) $R_{\sigma_r} = 9.7 \pm 0.8\,\mathrm{kpc}$ (or $R_{\sigma_r^2} = 4.8 \pm 0.4\,\mathrm{kpc}$).

These results are close to previous kinematic determinations of the scale lengths by Mayor (1974) ($R_\Sigma = 2.2\,\mathrm{kpc}$) or Oblak & Mayor (1987) ($R_{\sigma_r} = 10\,\mathrm{kpc}$ or $R_{\sigma_r^2} = 5\,\mathrm{kpc}$), Fux & Martinet (1994) ($R_\Sigma = 2.5\,\mathrm{kpc}$), and Bienaymé & Séchaud (1997) based on the local stellar kinematics.

We also constrain locally the rotation curve. Assuming $v_c(r) = r^\alpha$, we find $\alpha = -.24 \pm 0.04$.

In the frame of Stäckel potentials, we explicitly determine the dependence between vertical and horizontal motions. We show that the marginal velocity distribution of tangential and vertical velocities $f(v_\theta, v_z)$ allows us to constrain the shape of potential in the solar neighbourhood through the parameter $z_o$ (focus of the coordinate system associated to the fitted Stäckel potential) or $\Lambda$ (Eq. 13).

From 3D-velocity data, we measure $z_o = 5.7 \pm 1.4\,\mathrm{kpc}$ or $\Lambda = 0.69 \pm 0.10$. That quantity is linked to the total mass gradient in the galactic plane. It favours a spherical dark halo or flattened halos with a local thickness larger than $2\,\mathrm{kpc}$. More data would allow us to refine this determination. An extremely flat dark halo with all the mass in the galactic plane is ruled out. This conclusion confirms the results obtained measuring $K_z$, the force perpendicular to the galactic plane, and the local mass density (Crézé et al., 1998), a determination based on vertical motions and vertical density distribution of tracer stars. It is consistent with preliminary results from Ibata et al. (1998) based on the kinematics of the stream associated to the Sagittarius dwarf galaxy through the halo.

*Acknowledgements.* I would like to thank F. Ochsenbein, E. Chereul, C. Pichon and J. Pando for their help and comments.

## Appendix A: Disc distribution function in Stäckel potentials

### *A.1. Stäckel potentials*

A description of 3D Stäckel potentials is detailed in de Zeeuw (1985). Stäckel potentials are more tractable in confocal spheroidal coordinates. The prolate spheroidal coordinates $(\lambda, \theta, \nu)$ are related to the cylindrical coordinates $(r, \theta, z)$ by

$$r^2 = \frac{(\lambda+\alpha)(\nu+\alpha)}{\alpha-\gamma} \text{ and } z^2 = \frac{(\lambda+\gamma)(\nu+\gamma)}{\gamma-\alpha} \tag{A1}$$

$\alpha$ and $\gamma$ determine the shape of the coordinate surfaces, and $\lambda$, $\nu$ satisfies $-\gamma \leq \nu \leq -\alpha \leq \lambda$. Surfaces of constant $\lambda$ are spheroids and those of constant $\nu$ are hyperboloids. They all share the same foci located on the $z$ axis at $\pm z_o = \pm(\gamma-\alpha)^{1/2}$. In the limit $z_o \to \infty$, the coordinate system is cylindrical, and for $z_o \to 0$ it is spherical.

Then, the potential takes the form

$$\Phi(\lambda, \nu) = \frac{h(\lambda) - h(\nu)}{\lambda - \nu} \tag{A2}$$

where $h$ is an arbitrary function ($h(\lambda)$ and $h(\nu)$ are not defined on the same interval).

Properties of orbits in such potentials are discussed by de Zeeuw (1985). They all have three integrals of motions, for instance:

$$E = \Phi(\lambda, \nu) + \frac{1}{2}(r\dot{\theta})^2 + \frac{1}{2}\dot{r}^2 + \frac{1}{2}\dot{z}^2 \tag{A3}$$

$$L_z = r^2\dot{\theta} = r v_\theta \tag{A4}$$

$$\begin{aligned} I_3 = \Psi(\lambda, \nu) &- \frac{1}{2}\frac{z^2}{\gamma-\alpha}(\dot{r}^2 + (r\dot{\theta})^2) \\ &- \frac{1}{2}(\frac{r^2}{\gamma-\alpha} + 1)\dot{z}^2 + \frac{rz\dot{r}\dot{z}}{\gamma-\alpha} \end{aligned} \tag{A5}$$

with

$$\Psi(\lambda, \nu) = \frac{(\nu+\gamma)h(\lambda) - (\lambda+\gamma)h(\nu)}{(\gamma-\alpha)(\lambda-\nu)}. \tag{A6}$$

$I_3$ is also the vertical energy $E_z$ when the coordinate system is cylindrical, i.e. $z_o = \infty$.

*A.2. 3D disc distribution function*

In a context similar to this paper, i.e., an analysis of a stellar velocity distribution, Statler (1989) used Stäckel potentials and built a distribution function valid towards the galactic pole. He showed that the change of the orientation of the velocity ellipsoid may bias the estimated dynamical mass in the disc up to 10 percent for samples at a distance of $1\,\mathrm{kpc}$ from the galactic plane. Analytic axisymmetric galaxy models with three integrals of motion are also described by Dejonghe & de Zeeuw (1988).

Here, we give a 3D stellar disc distribution function that has nearly a Schwarzschild distribution behaviour in the limit of small dispersions. This distribution has also a density which is nearly radially exponential.

The distribution function is

$$f(E,L_z,I_3)=\frac{2\Omega(R_c)}{2\pi\kappa(R_c)}\frac{\Sigma(L_z)}{\sigma_r^2(L_z)}\exp\left[-\frac{E-E_{circ}}{\sigma_r^2}\right]\frac{1}{\sqrt{2\pi}}\frac{1}{\sigma_z(L_z)}exp\left\{-(\frac{R_c(L_z)^2}{z_o^2}+1)^{-1}(\frac{1}{\sigma_z^2}-\frac{1}{\sigma_r^2})I_3\right\} \tag{A7}$$

and depends on integrals of motion.

This can be written differently as:

$$\begin{aligned} f(E,L_z,I_3) &= f_{3D}(r,z;\dot r,\dot\theta,\dot z)\\ &= f_{//}(r;\dot r,\dot\theta)\frac{1}{\sqrt{2\pi}\sigma_z}f_\perp(r,z;\dot\theta,\dot z)\end{aligned} \tag{A8}$$

with

$$f_{//}(r;\dot r,\dot\theta)=\frac{2\Omega}{2\pi\kappa}\frac{\Sigma}{\sigma_r^2}\exp\left[-\frac{E_{//}-E_{circ}}{\sigma_r^2}\right] \tag{A9}$$

where $E_{//}=\Phi+\frac{1}{2}(v_r^2+v_\theta^2)$ (when z=0, the expression of $f_{//}$ is exactly that of $f_{2D}$, i.e. the 2D distribution function in Bienaymé & Séchaud, 1997) and with

$$f_\perp(r,z;\dot\theta,\dot z)=\exp\left\{-\frac{1}{2}\frac{\dot z^2}{\sigma_r^2}-(\frac{R_c(L_z)^2}{z_o^2}+1)^{-1}(\frac{1}{\sigma_z^2}-\frac{1}{\sigma_r^2})I_3\right\}. \tag{A10}$$

Properties of $f_{3D}$ are similar to $f_{2D}$, their density and kinematics having nearly exponential radial decreases.

The distribution function simplifies when $z=0$, (i.e., $\nu=-\gamma$). Adding an arbitrary constant to $h$ leaves the potential unchanged, so without loss of generality, we may put $h(-\gamma)=0$, then:

$$\Phi(\lambda,\nu=-\gamma) = \frac{h(\lambda)}{\lambda+\gamma} \tag{A11}$$

$$\Psi(\lambda,\nu=-\gamma) = 0 \tag{A12}$$

$$I_3(z=0) = -\frac{1}{2}(\frac{r^2}{z_o^2}+1)\dot z^2 \tag{A13}$$

and finally we obtain:

$$f_\perp=\exp\left\{-\frac{\dot z^2}{2\sigma_r^2}\left[1+(\frac{\sigma_r^2}{\sigma_z^2}-1)\left(\frac{r^2+z_o^2}{R_c(L_z)^2+z_o^2}\right)\right]\right\} \tag{A14}$$

In the case of a cylindrical potential, radial and perpendicular motions are uncoupled and $z_o=\infty$, so

$$f_\perp=\exp\left\{-\frac{\dot z^2}{2\sigma_z^2}\right\}. \tag{A15}$$

For a spherical potential (i.e., $z_o=0$) and a flat rotation curve $v_c(r)=v_o$, so $R_c=L_z/v_c$ and

$$f_\perp=\exp\left\{-\frac{\dot z^2}{2}\left[\frac{1}{\sigma_r^2}+(\frac{1}{\sigma_z^2}-\frac{1}{\sigma_r^2})\frac{v_o^2}{v^2}\right]\right\}. \tag{A16}$$

For a spherical potential ($z_o=0$) and a power law rotation curve $v_c(r)=v_o(r/R_0)^\alpha$. If $r=R_0$, we have

$$f_\perp=\exp\left\{-\frac{\dot z^2}{2}\left[\frac{1}{\sigma_r^2}+(\frac{1}{\sigma_z^2}-\frac{1}{\sigma_r^2})\left(\frac{v_o}{v}\right)^{2/(1+\alpha)}\right]\right\}. \tag{A17}$$

Finally, we remark the two following simplifications where the marginal distributions does not depend on $z_o$:

-Firstly, for motions in and parallel to the galactic plane ($v_z=0$, $z=0$ and $I_3=0$) we have

$$\begin{aligned} f_{3D}(r,z=0;v_r,v_\theta,&v_z=0) =\\ &f_{//}(r;v_r,v_\theta)\frac{1}{\sqrt{2\pi}\sigma_z},\end{aligned} \tag{A18}$$

and secondly when $z=0$ and $v_\theta=v_c(r)$, then $R_c=r$ and

$$\begin{aligned} f_{3D}(r,z=0;v_r,v_\theta=v_c(r),v_z) =\\ f_{//}(r;v_r,v_\theta=v_c(r))\frac{1}{\sqrt{2\pi}\sigma_z}\exp\left\{-\frac{\dot z^2}{2\sigma_z^2}\right\}.\end{aligned} \tag{A19}$$

It is straightforward to integrate (Eqs. A18-19) over the radial velocities, then similar expressions are obtained for the marginal velocity distributions $f(v_\theta,v_z=0)$ and $f(v_\theta=v_c(r),v_z)$ used in Sect. 5.

*Remark:* It is the requirement that the radial density ($\int f d^3v$) must be nearly exponential that makes one introduce the term $(\frac{R_c(L_z)^2}{(\gamma-\alpha)}+1)$ in the second exponential of Eq. A7. It is also this term that introduces the peculiar dependence in Eqs. A16 or A17 instead of having the uncoupled expression of Eq. A15. If the density were different, the coupling in A16-17 would be different.

## References


Amendt P., Cuddeford P., 1991, ApJ 368, 79

Bienaymé O., Séchaud N., 1997, A&A 323, 781

Binney J., Dehnen W., et al., 1997, Hipparcos-Venice'97, ESA SP-402, p473

Binney J., Tremaine S., 1987, Galactic dynamics. Princeton University Press, Princeton, NJ

Chereul E., Crézé M., Bienaymé O., 1997, Hipparcos-Venice'97, ESA SP-402, p545

Chereul E., Crézé M., Bienaymé O., 1998, A&A in press

Crézé M., Chereul E., Bienaymé O., Pichon C., 1998, A&A 329, 920

Cuddeford P., Amendt P., 1991, MNRAS 253, 427

Cuddeford P., Amendt P., 1992, MNRAS 256, 166

Cuddeford P., Binney J., 1994, MNRAS 266, 273
Dehnen W., 1998, AJ 115, 2384
Dehnen W., Binney J., 1998, MNRAS 298, 387
de Jong R.S., 1996, A&A 313, 377
Dejonghe H., de Zeeuw P.T., 1988, ApJ 333, 90
de Zeeuw P.T., 1985, MNRAS 216, 273
Eadie W.T., Drijard D., James F., et al., 1971, Statistical Methods in Experimental Physics. North-Holland
ESA, 1992, The Hipparcos Input Catalogue. ESA SP-1136
ESA, 1997, The Hipparcos Catalogue. ESA SP-1200
Evans N.W., Collett J.L., 1993, MNRAS 264, 353
Feast M., Whitelock P., 1997, MNRAS 291, 683
Figueras F., Gómez A.E., et al., 1997, Hipparcos-Venice'97, ESA SP-402, p519
Fux R., Martinet L., 1994, A&A 287, L21
Gliese W., Jahreiss H., 1991, Preliminary Version of the Third Catalogue of Nearby Stars, on The NASA/ADC and CDS
Gómez A.E., Grenier S., et al., 1997, Hipparcos-Venice'97, ESA SP-402, p621
Hori G., Liu T., 1963, PASJ 15, 100
Ibata R., et al., 1998, private communication
Kamper K.W., Kang Min Kim, Thomson J.R., 1997, Balt. Astron. 6, 111
Kendall M.G., Stuart A., 1967, The advanced theory of statistics. Vol. 2, C. Griffin & Co, London
Kent S.M., Dame T.M., Fazio G., 1991, ApJ 378, 131
Kent S.M., de Zeeuw T., 1991, AJ 102, 1994
Kovalesky J., Lindegren L., Perryman M.A.C., et al., 1997, A&A 323, 620
Kuijken K., Dubinski J., 1995, MNRAS 277, 1341
Kuijken K., Tremaine S., 1991, In: Sundelius B. (ed.) Dynamics of discs galaxies. Univ. Press, Göteborg, 71
Lewis J.R., Freeman K.C., 1989, AJ 97, 139
Mayor M., 1974, A&A 32, 321
Neese C.L., Yoss K.M., 1988, AJ 95, 463
Nemec J., Nemec A.L., 1991, PASP 103, 95
Oblak E., Mayor M., 1987, European Regional Astronomy Meeting of the IAU, 10th, Proceedings. Vol. 4, 263
Ojha D.K., Bienaymé O., et al., 1996, A&A 311, 456
Olling R.P., Merrifield M.R., 1998, MNRAS 297, 943
Porcel C., Garzón F., et al., 1998, A&A 330, 136
Reid I.N., Hawley S.L., Gizis J.E., 1995, AJ 110, 1838
Reid M.J., 1993, ARA&A 31, 345
Robin A.C., Crézé M., Mohan V., 1992, A&A 265, 32
Rohlfs K., Kreitschmann J., 1988, A&A 201, 51
Ruphy S., Robin A.C., et al., 1996, A&A 313, L21
Shu F.H., 1969, ApJ 158, 505
Siegel M.H., Majewski S.R., Reid I.N., Thompson I., 1997, Proper motions and galactic astronomy. ASP Conf. Ser. 217, p175
Statler T.S., 1989, ApJ 344, 217
Upgren A.R., Harlow J.J.B., 1996, PASP 108, 64
van de Hulst H.C., 1962, Bull. Astr. Inst. Neth. 16, 235
Vyssotsky A.N., 1963, In: Strand K.A. (ed) Basic Astronomical Data. Univ. Chicago Press, Chicago, 192
Warren M.S., Quinn P.J., et al., 1992, ApJ 399, 405
Weiss E.W., Upgren A.R., 1995, AJ 109, 812